EurJIC
European Journal of Inorganic Chemistry

Research Article
doi.org/10.1002/ejic.202300749

Chemistry Europe
European Chemical Societies Publishing

www.eurjic.org

Solvent and Dihalide Substituent Effects on Crystal Structure, Spin-Crossover Behavior and Conductivity of the Cationic Mn(III) Complexes with Electroactive TCNQ Counteranions

Aleksandra V. Tiunova,[a, b] Denis V. Korchagin,*[a] Anna V. Kazakova,*[a] Gennady V. Shilov,[a] Lev I. Buravov,[a] Aleksei I. Dmitriev,[a] Mikhail V. Zhidkov,[a] Vladimir N. Zverev,[c] Eduard B. Yagubskii,*[a] and Sergei M. Aldoshin[a]

Cationic Mn(III) complexes with 3,5-Hal-sal$_2$323 (Hal=diCl, diBr, BrCl) ligands containing electroactive TCNQ anions as counterions have been synthesized: [Mn(3,5-diCl-sal$_2$323)](TCNQ)$_2$ (**1**), [Mn(3,5-diBr-sal$_2$323)]$_2$(TCNQ)$_3$·6CH$_3$CN (**2**), and [Mn(3,5-Br,Cl-sal$_2$323)]$_2$(TCNQ)$_3$·6CH$_3$CN (**3**). The crystal structures, magnetic and conducting properties of the obtained compounds have been investigated. In **1**, an incomplete spin transition from the low-spin (LS) state at 100 K to the high-spin (HS) state upon heating to 400 K is observed. Isostructural complexes **2** and **3** contain 6 molecules of solvated acetonitrile, which is lost upon heating, accompanied by the crystal structure transformation. As a result, desolvated complexes jump to the HS state. The temperature dependences of resistivity **2** and **3** show resistivity jumps associated with the loss of lattice solvent.

Introduction

The design and synthesis of multifunctional molecular materials combining two or more properties ((super)conductivity, magnetism, photochromism, nonlinear optical properties, etc.) is currently one of the most actively developing trends in the chemistry and physics of new materials.[1] The coexistence of different properties in the same crystal lattice and possible synergistic effects make multifunctional materials promising for application in new generation electronic devices and information systems. Such compounds allow to control one of the properties by influencing the other by external factors (temperature, light, magnetic field, pressure). Materials that combine conductivity and spin-crossover can become the basis for the development of molecular spintronics. To date, the number of such multifunctional systems is limited, and active research is underway in this direction. Most of them are based on spin-crossover cationic complexes Fe(II) and Fe(III) combining as counterions electroactive fractionally charged anions of tetra-
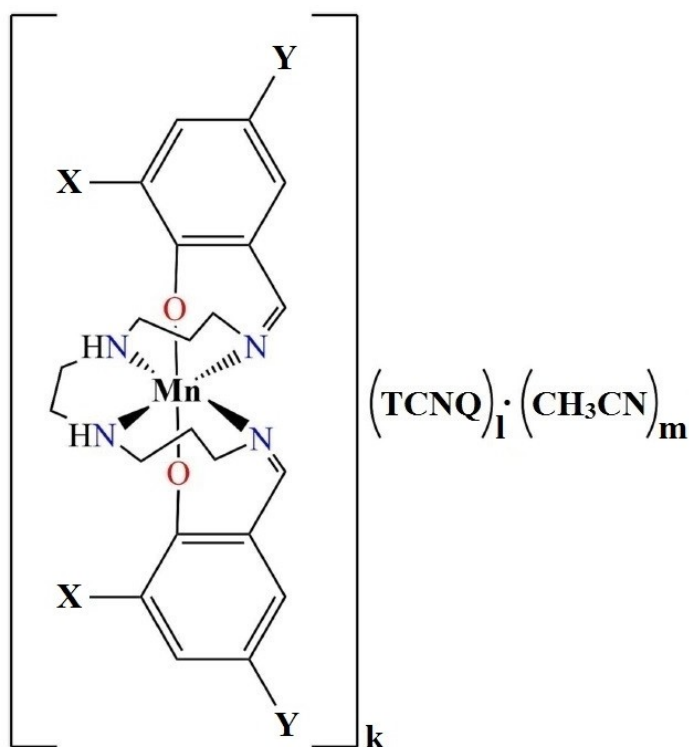
cyanoquinodimethane (TCNQ$^{\delta-}$) or [M(dmit)$_2$]$^{\delta-}$ ($0<\delta<1$; M=Ni, Pd; dmit=1,3-dithia-2-thione-4,5-dithiolate).[2–12] It is known that spin transitions are most characteristic of the d^7 (Co(II)), d^6 (Fe(III)) and d^5 (Fe(II)) systems in which two electrons switch between t$_{2g}$ and e$_g$ orbitals in the case of iron complexes.[13–15] In the 21st century, however, a class of spin-crossover cationic Mn(III) complexes (d^4 system) with the ligand sal$_2$323 (sal$_2$323 = N,N′-bis(3-(2-oxy-benzylideneamino)propyl)-ethylenediamine) and its derivatives was discovered, in which one electron is transferred between low-spin (LS, S=1) and high-spin (HS, S=2) states.[16–19] The sal$_2$323 ligand is a product of the condensation reaction of two molecules of salicylaldehyde with flexible tetraamine N,N′-bis(3-aminopropyl)ethylenediamine. The abbreviation 323 refers to the number of alkyl linkages in the starting tetraamine. A characteristic feature of the molecular structure of these six-coordination manganese complexes is the presence of oxygen atoms in the axial positions and four nitrogen atoms in the equatorial plane (Figure 1). The temperature-induced transition from the low-spin state to the high-spin state is accompanied by an increase in the manganese-nitrogen distances by 0.12–0.18 Å and a significant distortion of the coordination octahedron, while the manganese-oxygen distances remain practically unchanged.[17] The study of the influence of substituents in the phenolate ring, counterions and crystallization solvents on the spin-crossover behavior of the [Mn-(sal$_2$323)]$^+$ family complexes has led to several important results in recent years.[18,19] Complexes with sharp spin transitions exhibiting significant hysteresis have been synthesized,[20–27] including complexes in which stepwise spin transitions are associated with structural transitions.[25–27] In addition to temperature-induced spin transitions, some of these manganese complexes exhibit SCO effects in rather low magnetic fields starting even below 5T.[27,28] In 2019, we first synthesized a

Figure 1. [Mn(3,5-diCl-sal$_2$323)](TCNQ)$_2$ (**1**, X=Y=Cl, k=1, l=2, m=0), [Mn(3,5-diBr-sal$_2$323)]$_2$(TCNQ)$_3$·6CH$_3$CN (**2**, X=Y=Br, k=2, l=3, m=6), [Mn(3,5-Br,Cl-sal$_2$323)]$_2$(TCNQ)$_3$·6CH$_3$CN (**3**, X=Br,Y=Cl, k=2, l=3, m=6).

[Mn(5-Cl-sal$_2$323)]$^+$ complex with a fractionally charged anion of TCNQ, [Mn(5-Cl-sal$_2$323)]TCNQ$_{1.5}$·2CH$_3$CN, which showed a sharp spin transition with a 50 K width and semiconducting behavior.[29] In contract, the bromoisomorphic analog [Mn(5-Br-sal$_2$323)]TCNQ$_{1.5}$·2CH$_3$CN does not exhibit spin-crossover phenomena and remains in the high-spin state in the temperature range of 2–300 K.

In order to further investigate the influence of halide substituents in the phenolate ring of the ligand on the structure, SCO behavior and transport properties of [Mn^{3+}(sal$_2$323)] cationic complexes with TCNQ counteranions, we used dihalide derivatives of the sal$_2$323-ligand and synthesized the following compounds in the present work: [Mn(3,5-diCl-sal$_2$323)]$^+$(TCNQ)$_2$ (**1**), [Mn(3,5-diBr-sal$_2$323)]$_2$(TCNQ)$_3$·6CH$_3$CN (**2**) and [Mn(3,5-Br,Cl-sal$_2$323)]$_2$(TCNQ)$_3$·6CH$_3$CN (**3**) (Figure 1). Herein, we present the synthesis, crystal structures, magnetic and conducting properties of these complexes.

Results and Discussion

Synthesis

Complex **1** was synthesized as black plate-like crystals from a reaction between [Mn(3,5-diCl-sal$_2$323)]ClO$_4$ and a mixture of LiTCNQ and TCNQ in hot CH$_3$CN, while complexes **2** and **3** were obtained as black needle-like crystals from the same reaction using [Mn(3,5-diBr-sal$_2$323)]ClO$_4$ and [Mn(3,5-Br,Cl-sal$_2$323)]ClO$_4$, respectively (see Experimental). In contrast to **1**, complexes **2**

and **3** contain 6 molecules of lattice acetonitrile. Thermogravimetric analysis of **2** and **3** indicated weight losses of 8.16% and 11.32%, respectively, (calculated 10.4% for **2** and 11.3% for **3**), see Figures S1 and S2. The loss of solvent is accompanied by endothermic peaks around 96.5–104.3 °C (maximum at 100.9 °C) and 77.2–82.4 °C (maximum at 80 °C), respectively.

Crystal Structure

The crystal structure of **1** has been studied at four different temperatures (100, 200, 300 and 373 K). Compound **1** crystallizes in the triclinic system (space group *P-1*) with one whole and two halves of TCNQ molecules in general and special positions, respectively, per one [Mn(3,5-diCl-sal$_2$323)]$^+$ complex cation (Figure 2a), different TCNQ molecules further denoted as A (in the general position) and B, C (in special positions).

The crystal structures of **2** and **3** have been studied only at 100 K, since the quality of the crystals deteriorates greatly with increasing temperature of the X-ray diffraction experiments, making detailed analysis difficult. Compounds **2** and **3** are isostructural and crystallizes like **1** in the triclinic system (space group *P-1*), but with two [Mn(3,5-diHal-sal$_2$323)]$^+$ complex cations (Figure 2b), three TCNQ anions and six solvent molecules - MeCN in the general positions of asymmetric units. The presence of such a large number of molecules of a rather volatile solvent in the crystal structures of **2** and **3** is apparently the reason for the decrease in the quality of the crystals of the compounds under consideration.
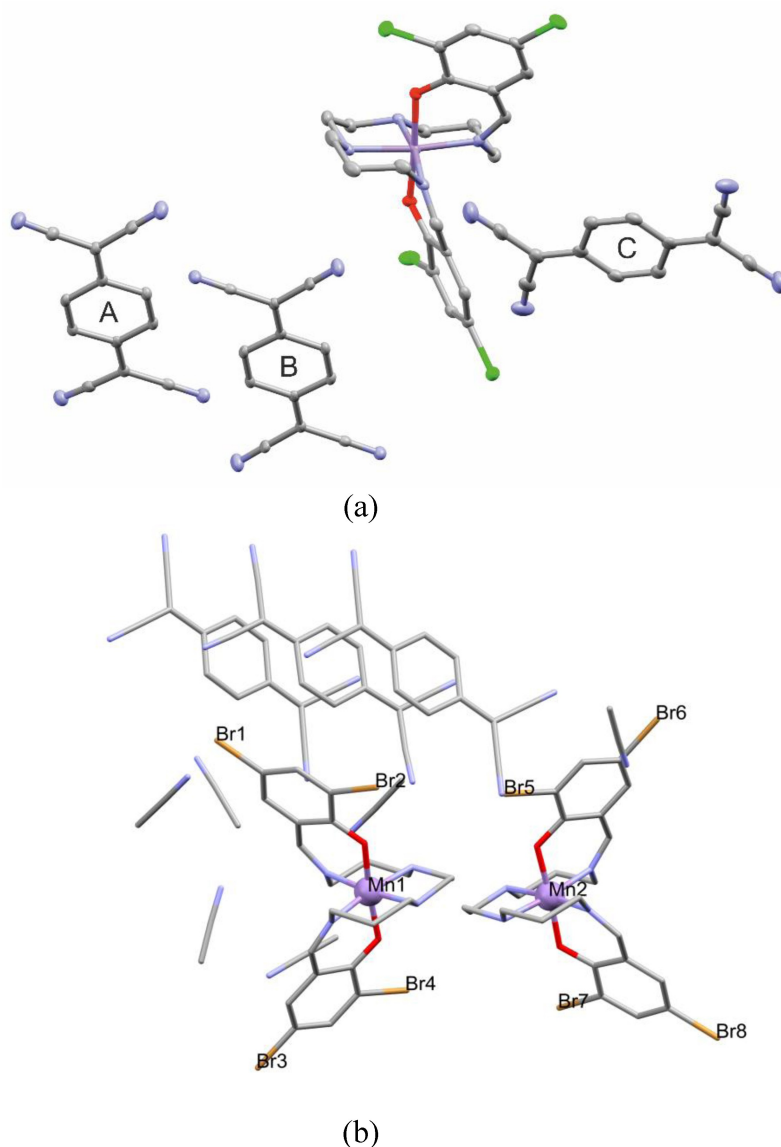
Figure 2. The general view of compounds **1** (a) and the asymmetric unit of **2** (b). Violet – Mn, green – Cl, orange – Br, red- O, blue – N, gray – C. H atoms are omitted for clarity.

The coordination environment of the Mn ion in **1** is completely distorted with compression along the O1-Mn–O2 bonds due to the Jahn-Teller effect. The Mn–N,O bond lengths and octahedral distortion parameters at different temperatures are listed in Table 1. The axial Mn–O bond lengths do not change significantly with increasing of temperature. At 100 and 200 K, the average equatorial bond lengths Mn–N_{im} and Mn–N_{am} in complex **1** are in the range of that expected for the LS Mn(III) ion.[17,18] At the same time, at 200 K, the Mn–N_{am} bond lengths are slightly larger than at 100 K, which may indicate the initial point of the spin transition of the manganese(III) ion to the HS state. When the temperature is increased to 300 K, the Mn–N bond lengths increase slightly, it means that only a small part of the LS Mn ions has been transited to the HS state (Table 1). A further increase the temperature to 373 K reveals an elongation of the Mn–N bond lengths, corresponding to an increase in the fraction of HS Mn ions in **1**, while these values do not reach those of Mn–N_{im} 2.12 and Mn–N_{am} 2.23 Å corresponding to the HS Mn(III) ion.[17,18]

The strong changes with temperature in the X–Mn-X angles are also observed, which is well illustrated by the octahedral distortion parameters (ODPs) (Σ and Θ) shown in Table 1. For complex **1**, the ODPs for Mn ions at 100 and 200 K are close and correspond to the LS state of the Mn(III) ion.[17,18] By increasing the temperature from 200 to 300 K, the values of the ODPs for Mn ions increase from ~36 to ~45 and from ~104 to ~130° for Σ and Θ, respectively. At 373 K, the octahedral distortion parameters for the Mn ion are equal to ~53 and ~157° for Σ and Θ, respectively. These parameters also have intermediate values between those for LS and HS Mn(III) ions within a higher proportion of HS Mn ions, indicating an incomplete gradual spin transition between LS (S = 1) and HS

EurJIC
European Journal of Inorganic Chemistry

Research Article
doi.org/10.1002/ejic.202300749

Chemistry Europe
European Chemical Societies Publishing

Table 1. Selected bond lengths and octahedral distortion parameters[a] in 1–3.

Compound	1				2[b]	3[b]
Param./Temp.	100 K	200 K	300 K	373 K	100 K	100 K
Mn—O, Å	1.866(1) 1.885(1)	1.865(1) 1.883(1)	1.861(2) 1.885(1)	1.866(2) 1.882(2)	1.881(5)/ 1.890(5)	1.893(6)/ 1.893(7)
Mn-N_{im}, Å	1.985(2) 1.990(2)	1.987(2) 1.990(2)	2.017(2) 2.030(3)	2.046(3) 2.064(3)	1.978(7)/ 1.979(7)	1.978(8)/ 1.980(7)
Mn-N_{am}, Å	2.038(2) 2.049(2)	2.049(2) 2.058(2)	2.081(3) 2.114(3)	2.119(3) 2.157(3)	2.045(7)/ 2.034(7)	2.049(8)/ 2.038(8)
Σ, °	35.0	36.0	45.1	53.3	30.3/25.4	28.4/24.2
Θ, °	101.4	103.9	130.1	157.0	86.0/73.4	77.8/69.7
ζ, Å	0.376	0.392	0.499	0.594	0.350/0.311	0.327/0.309

[a] Σ is the sum of the deviation from 90° of the 12 cis-angles in the coordination polyhedron. Θ is the sum of the deviation from 60° of the 24 trigonal angles of the projection of the octahedron onto the trigonal faces. ζ is the sum of deviation from individual M–N(or O) bond distances with respect to the mean M–X bond distance (the distance distortion parameter). [b] the average values for two non-equivalent Mn(III) ions.

(S = 2) states of Mn(III) ion in complex **1**. At 100 K, both Mn(III) ions in **2** and **3** are in LS states,[17,18] based on the equatorial bond lengths Mn–N and ODPs (Table 1).

In crystal structure **1**, the [MnL]⁺ cationic complexes are packed in pairs, but there are no shortened intermolecular interactions between them (black, Figure 3a). Two crystallographically independent TCNQ anions (A and B) form the stacks along the crystallographic direction *b* (red and light green, Figure 3). The pronounced dimerization of the stacked TCNQ anion molecules A is observed within a much smaller interplanar distance (3.16 Å). Dimers of TCNQ A molecules

alternate in the stacks with the other two strongly displaced TCNQ molecules (B), with an interplanar distance between A and B of ~3.53 Å (Figure 3b). Both overlaps A–A and A–B are of the ring-over-bond type with longitudinal and transverse displacement,[30,31] respectively (Figures S3a and b). The TCNQ molecules B also form centrosymmetric dimers but in the plane due to C–H(B-TCNQ)…N(B-TCNQ) 2.43 Å pairwise interactions. The third crystallographically non-equivalent anion TCNQ (C) is arranged separately surrounded by [MnL]⁺ cations. (blue, Figure 3) and forms planar chains via C–H(C-TCNQ)…N(C-TCNQ) 2.66 Å interactions (Figure S3c). It is interesting to note that the
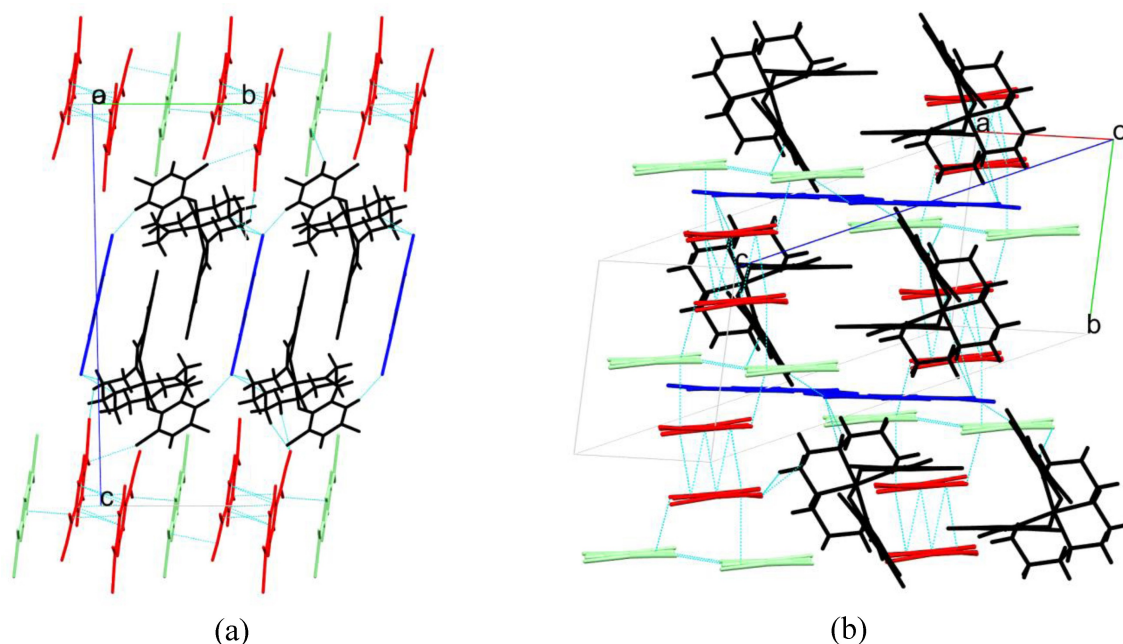
Figure 3. Projection of fragment of the crystal structure of **1** onto the *bc* plane (a), the crystal packing of **1** viewed from the side relative to the direction of TCNQ stacks (b). TCNQ anions (A – red, B – light green and C - blue) and [MnL]⁺ cations (black) are shown by different colors. Dash cyan lines show the short intermolecular contacts.

EurJIC
European Journal of Inorganic Chemistry

Research Article
doi.org/10.1002/ejic.202300749

Chemistry Europe
European Chemical
Societies Publishing

planes of TCNQ anions C and the phenyl rings of the cationic complexes $[MnL]^+$ line up in parallel with interplanar distances of 3.38 and 2.83 Å, respectively, (Figure 3a). The π-system of the TCNQ anions C and the phenyl ring of one of the complex cations overlap, while the phenyl rings of the cations in the dimers do not overlap when projected onto each other's planes. In addition to purely electrostatic interactions, short intermolecular contacts between anions and cations are observed in crystal structure **1**. The complex cations in **1** are strongly bound to the TCNQ anions C by the intermolecular hydrogen bond N–H…N (d(H…N) = 2.24 Å, d(N…N) = 2.97 Å, <NHN = 142.5°) and the shortened contact C–H(MnL^+)…N(C-TCNQ) 2.34 Å. The interaction of the $[MnL]^+$ cations with two other crystallographically independent molecules B and A TCNQ C–H(MnL^+)…N(TCNQ) 2.54 and 2.59–2.62 Å, respectively, is much weaker.

It was previously shown that the charge state of TCNQ can be estimated from the length of its carbon-carbon bonds[32] (Table 2). Using the Kistenmacher relationship, the charge distribution for TCNQ anions in the crystal structure **1** was estimated. Thus, the TCNQ A molecule, which is part of the dimer, has a charge of −0.5e, the dimers alternate in stacks with a practically neutral molecule TCNQ B (−0.2e). The TCNQ C molecule, located separately, has a large negative charge (−0.8e). The total charge on the four TCNQ species is −2.0, which is consistent with the +1 charge on one of two $[MnL]^+$ cations. The strong localization of the charge in the stacks and the displacement of some molecules relative to the stack lead to the semiconductor nature of the conductivity of compound **1** (see below). Using the same approach and taking into account the accuracy of the determined lengths of the C–C bonds in TCNQ anions due to the quality of the crystals **2** and **3**, we can only say that these anions carry approximately the same charge in **2** (Table 2). Considering the low accuracy in determining the C–C bond lengths due to the poor quality of the single crystals **3**, it does not make sense to estimate the charges of the TCNQ molecules in this complex using the Kistenmacher ratio. It can only be noted that given the isostructural character of compounds **2** and **3**, as well as the proximity of their conductive and magnetic properties (see below), we can expect a similar charge distribution of between the TCNQ molecules in structures **2** and **3**.
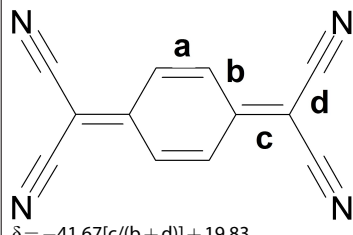
In **2** and **3**, there are also no shortened intermolecular interactions between adjacent $[MnL]^+$ cations as in **1** (black, F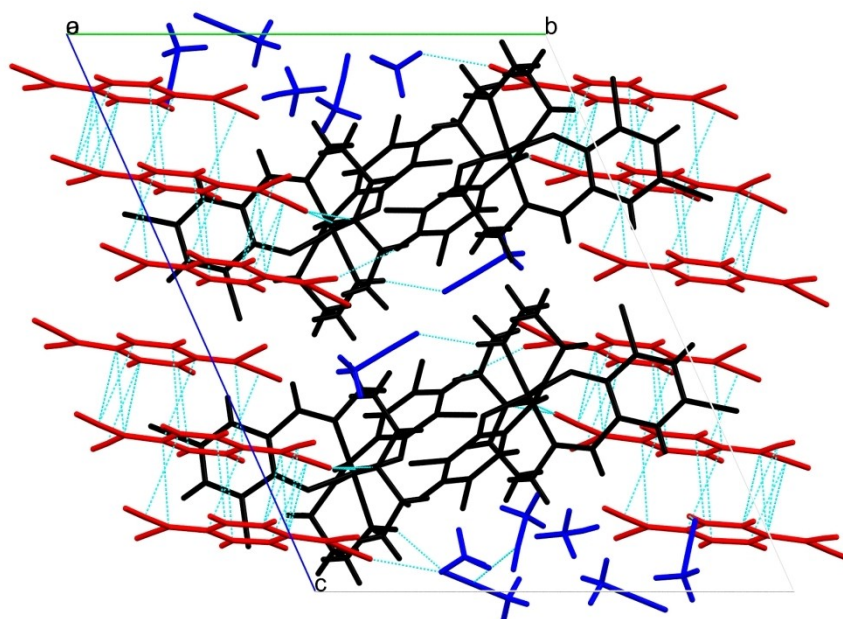igure 4). TCNQ anions do not form continuous stacks in the crystal structure of compounds **2** and **3**. All three crystallographically non-equivalent TCNQ anions pack in triads with interplanar distance 3.04 Å, the two triads form a single block (red, Figures 4 and S4d). Moving from one triad to another inside the block, a shift in the center of the TCNQ molecule and an increase in the interplanar distance by 3.33 Å between the planes of the molecules of adjacent triads are observed (Figures 4 and S4d). Both in and between triads inside the block the TCNQ molecules overlaps are of the ring-over-bond type with longitudinal and longitudinal-transverse displacement, respectively (Figures S4a and b). There is no continuous overlap of the π-orbitals of TCNQ molecules from adjacent blocks (Figures S4c and e). The solvent molecules can be divided into two groups, one MeCN molecule is weakly H-bonded to the $[MnL]^+$ cation (d(H…N) = 2.26 Å, d(N…N) = 3.08 Å, <NHN = 138.3°) and the other five molecules are located in the cavity and are weakly bonded in the crystal structure. This circumstance is probably the reason for the low stability and the quality of the single crystals of compounds **2** and **3**. The central TCNQ molecule of the triad in **2** has an strong N…H–N H-bond with the $[MnL]^+$ cation (d(H…N) = 1.97 Å, d(N…N) = 2.91 Å, <NHN = 154.3°).

Magnetic Properties

The temperature dependences of magnetic susceptibility ($χ_m$) of freshly filtered polycrystalline samples of complexes **1**, **2** and **3** were investigated at temperature range of 2–400 K in heating and cooling modes under an applied field of 0.5 T. Complex **1** exhibited a gradual and incomplete SCO in both modes without any hysteresis (Figure 5a). The $χ_mT$ value is 2.5 cm^{3}K/mol at 400 K, which is slightly lower than the theoretical value of $χ_mT$ (3.0 cm^{3}K/mol) for the HS Mn(III) ion with S = 2 and g = 2, indicating that ~80% of the sample undergoes the temperature-driven LS→HS conversion by 400 K. This result correlates well with the data of X-ray analysis, which show an increase in Mn-N$_{am}$ and Mn-N$_{im}$ bond lengths and distortion parameters of the coordination octahedron starting from 200 K, which is related to the transition from the LS to the HS state. With decreasing temperature, the $χ_mT$ decreases to a plateau of 1.35 cm^{3}K/mol below 200 K. This low-temperature $χ_mT$ value is slightly higher than expected for LS Mn(III) ion (S = 1, $χ_mT$ = 1.00 cm^{3}K/mol). This deviation may be caused by weak para-

Table 2. The charges (δ) of different TCNQ anions in **1–3** estimated from Kistenmacher's relationship.

$$\delta = -41.67[c/(b+d)] + 19.83$$

Species	a	b	c	d	c/b+d	δ
TCNQ^0	1.346	1.448	1.374	1.440	0.476	0.0
TCNQ$^{-0.5}$	1.354	1.434	1.396	1.428	0.488	−0.5
TCNQ^{-1}	1.373	1.423	1.420	1.416	0.500	−1.0
TCNQ (**1A**)	1.353	1.433	1.399	1.431	0.488	**−0.50**
TCNQ (**1B**)	1.348	1.438	1.382	1.434	0.481	**−0.20**
TCNQ (**1C**)	1.354	1.421	1.408	1.415	0.496	**−0.83**
TCNQ (**2A**)	1.346	1.440	1.407	1.437	0.489	**−0.55**
TCNQ (**2B**)	1.351	1.437	1.394	1.421	0.488	**−0.50**
TCNQ (**2C**)	1.362	1.436	1.399	1.426	0.489	**−0.55**

EurJIC
European Journal of Inorganic Chemistry

Research Article
doi.org/10.1002/ejic.202300749

**Chemistry
Europe**
European Chemical
Societies Publishing

Figure 4. Projection of fragment of the crystal structure of **2** onto the *bc* plane. TCNQ anions – red, [MnL]⁺ cations (black) and solvent MeCN molecules (blue) are shown by different colors. Dash cyan lines show the short intermolecular contacts.
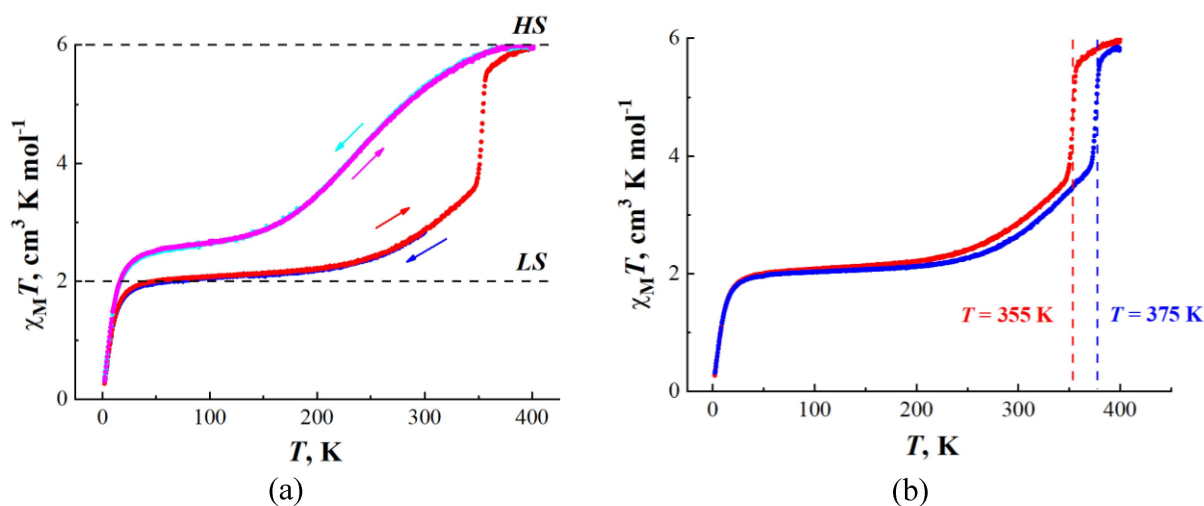

(a)

(b)
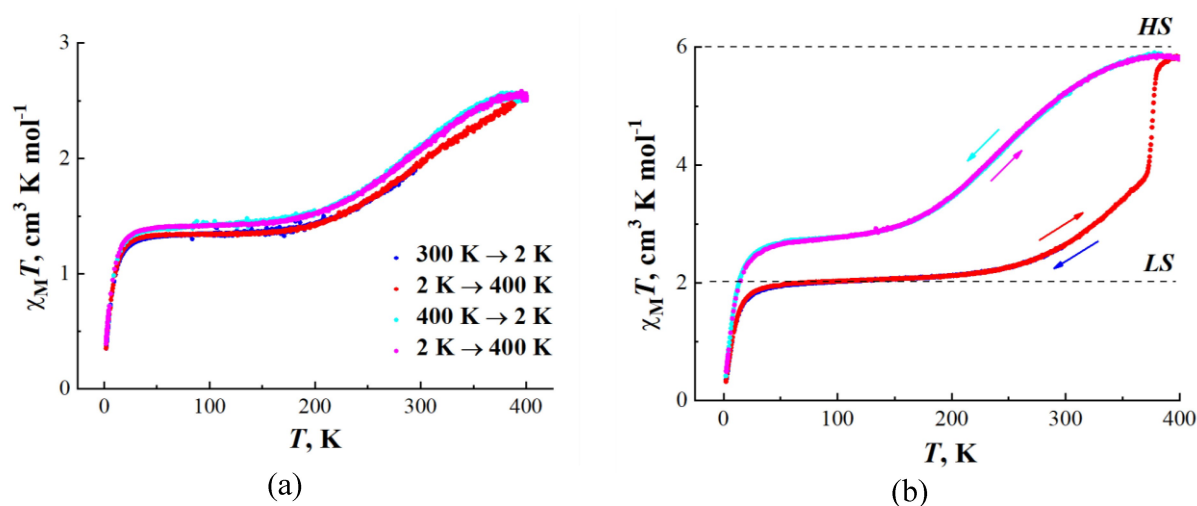
Figure 5. (a) The temperature dependences of the $\chi_m T$ product for complex **1**. (b) Temperature dependences of the $\chi_m T$ for **2** measured in the cooling and warming modes. Blue symbols are the first cooling from 300 K to 2 K. Red symbols are the first warming from 2 K to 400 K. Cyan symbols - second cooling from 400 K to 2 K. Magenta symbols - second warming from 2 K to 400 K.

magnetic contribution from the fractionally charged TCNQ$^{\delta-}$ anions as observed in Ref.[11] When the temperature is further reduced to about 30 K, the $\chi_m T$ decreases sharply, reaching a value of 0.36 cm³K/mol at 2.K (Figure 5a). The sharp drop in $\chi_m T$ at temperatures below 50 K is characteristic for the complexes of the [Mn(sal₂323)]⁺ family and is due to zero-field splitting effects for the Mn(III) ion.

Isostructural complexes **2** and **3** show a similar magnetic behavior (Figure 5b, 6a). Upon cooling from 300 K, the $\chi_m T$ value begins to decrease slowly below 240 K, reaching 2.03 and 2.08 cm³K/mol for **2** and **3**, respectively, in the broad plateau region of 50–200 K. The observed $\chi_m T$ values correspond to the

theoretical $\chi_m T$ value for the two Mn(III) ions in the low-spin state, which correlates well with the results of X-ray analysis for both complexes. With an increase in temperature from 240 K, a gradual increase in the $\chi_m T$ value is observed up to temperatures of 375 K and 355 K, at which sharp jumps in $\chi_m T$ occur in **2** and **3**, respectively (Figure 6b). Upon further heating to 400 K, $\chi_m T$ values reach saturation by 6.0 cm³K/mol, which is consistent with the expected value for two Mn(III) ions in the HS state. Upon cooling from 400 to 2 K, gradual spin transitions from HS in LS states below 100 K are observed for both complexes. The curves recorded in the cooling and heating modes coincide. The values of $\chi_m T$ at 100 K (2.78 and 2.64 cm³K/mol for **2** and **3**,

Eur. J. Inorg. Chem. **2024**, e202300749 (6 of 11)

© 2024 Wiley-VCH GmbH

EurJIC
European Journal of Inorganic Chemistry

Research Article
doi.org/10.1002/ejic.202300749

Chemistry Europe
European Chemical Societies Publishing

Figure 6. (a) Temperature dependences of the $\chi_m T$ for **3** measured in cooling and warming modes. Blue symbols - first cooling from 300 K to 2 K. Red symbols - first warming from 2 K to 400 K. Cyan symbols second cooling from 400 K to 2 K. Magenta symbols - second warming from 2 K to 400 K. (b) Temperature dependences of the $\chi_m T$ for **2** (blue symbols) and **3** (red symbols) measured at the first warming from 2 K to 400 K. The crystal structure transformation temperature determined from the maximum of the derivative $d(\chi_m T)/dT$ is 375 and 355 K for **2** and **3**, respectively.

respectively) are somewhat higher than would be expected for the two Mn(III) ions in the LS state. The jumps in $\chi_m T$ at elevated temperatures are related to the loss of lattice solvent at these temperatures, as follows from the analysis of the thermogravimetric and DSC curves for both complexes (Figures S1, S2, S5). The loss of solvent is accompanied by the crystal structure transformation. Powder X-ray diffraction after heating complexes **2** and **3** in a magnetometer chamber to 400 K shows that the crystallinity of the desolvated samples is preserved (Figure S6), their diffraction patterns are close to each other and become significantly different from those calculated from the crystal structure of solvated isostructural complexes **2** and **3** (Figure S6). The IR spectra of the desolvated samples are almost identical and differ markedly from the IR spectra of the parent complexes (Figures S7–S13). It is interesting to note that the dependences of $\chi_m T$ vs T for **2** and **3** after heating to 400 K and subsequent storage in air for one month coincide (Figure S14). Thus, it can be assumed that these new structures of complexes do not absorb water from air after desolvation. We have not been able to resolve the structures of desolvated complexes because solvent loss results in disintegration of the crystals. Heating of selected crystals **2** and **3** in the diffractometer chamber or under vacuum resulted in strong deterioration of crystal quality.

Transport Properties

The temperature dependence of the resistance R for the complex **1** is presented in the Figure 7. The value of the conductivity σ at room temperature measured along the TCNQ—C chains (axis *a*) is $5 \cdot 10^{-5}$ Ohm$^{-1} \cdot$cm^{-1}. As seen from the Insert to the Figure 7, the sample resistance depends exponentially on the temperature with the characteristic activation energy $\Delta = 222$ meV.

The TCNQ—C chains in structure **1** are built from TCNQ anions with charge close to −1, which leads to strong electron-electron repulsion; the σ-π interactions existing in these chains also do not favor conductive pathways. Therefore, it is quite expected that crystals **1** have low conductivity. The conductive paths along the *b*-axis, i.e., in the direction of the TCNQ stacks consisting of independent molecules A and B, also lack, since there is a strong charge localization in these stacks: they are constructed from TCNQ-A$^{0.5}$- TCNQ-A$^{0.5}$-dimers separated by dimers of almost neutral TCNQ—B molecules. Electrical transport in organic molecular conductors depends crucially on the magnitude of the transfer integral, which is proportional to the overlap of intermolecular orbitals.[33,34] Typically, in the case of highly ($\sigma_{300K} \sim 50$–100 Ohm$^{-1} \cdot$cm^{-1}) and moderately ($\sigma_{300K} \sim 1.0$ Ohm$^{-1} \cdot$cm^{-1}) conductive fractionally charged TCNQ salts, the crystals grow as long thin needles or elongated plates along the shortest crystallographic axis, respectively, with the long direction corresponding to the stack propagation, which also coincides with the direction of greatest conductivity.[35,36] The habit of TCNQ salt crystals reflects the structure of their stacks and thus the conductivity.

The $R(T)$ dependences for isostructural complexes **2** and **3** are shown in the Figures 8 and 9, respectively. The value of the conductivity at room temperature measured in the *ac* plane (along the *a*-axis) is $1 \cdot 10^{-5}$ Ohm$^{-1} \cdot$cm^{-1} for **2** and $7 \cdot 10^{-6}$ Ohm$^{-1} \cdot$cm^{-1} for **3**. The conductivity values are typical of low conductivity TCNQ salts, which do not show conductivity anisotropy, in contrast to the observations for higher conductivity TCNQ salts.[35] In **2**, **3**, the anionic subsystem in the *ac*-plane is built from single blocks of TCNQ molecules that do not overlap with each other and there are no shortened contacts between them.

The temperature dependences of the resistance look quite differently for **2** and **3** with respect to that of **1**, because at high temperature these complexes lose the lattice solvent, the loss
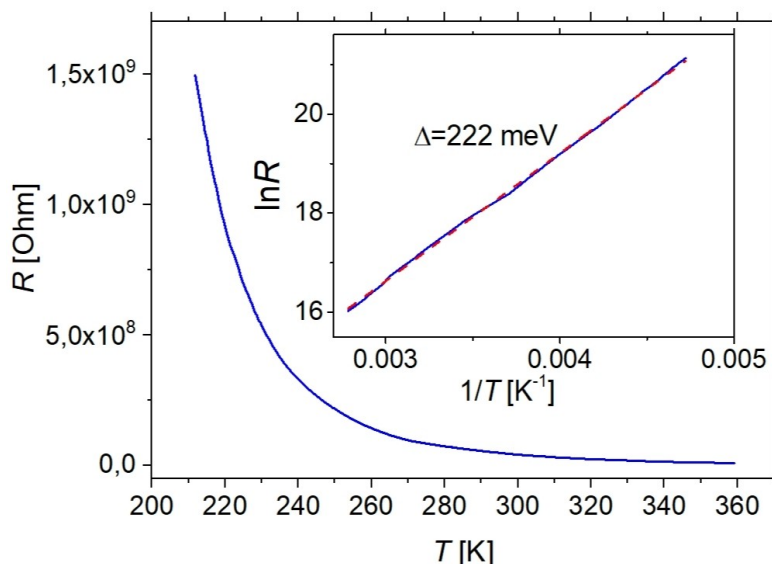
Eur. J. Inorg. Chem. **2024**, e202300749 (7 of 11)

© 2024 Wiley-VCH GmbH

Figure 7. The temperature dependence of the resistance R for the sample of complex **1**. The Arrhenius plot is presented in the Insert.
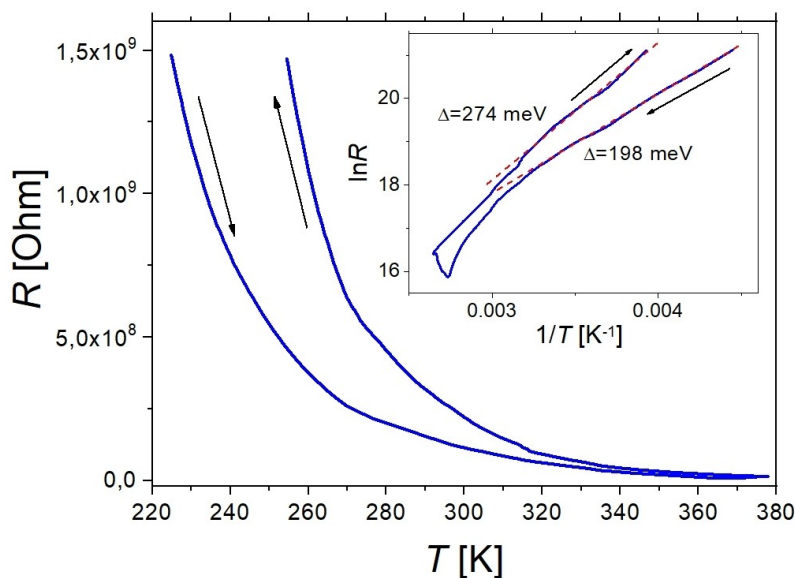

Figure 8. The temperature dependence of the resistance R for the sample of complex **2**.

of which is accompanied by the crystal structure transformation. That is why the R(T) dependences for **2** and **3** show resistance jumps (Figures 8 and 9), which correlate with jumps on the $\chi_m T$ vs T dependences for **2**, **3**.

It can be seen from Figures 8 and 9 that for both complexes, as the temperature rises, $R(T)$ depends exponentially on the temperature, as shown by the Arrhenius plots presented in the insets. However, at T > 300 K, the $R(T)$ dependences deflect from the exponential one towards the lower resistance. Then, at ~360 K for **2** and at ~335 K for **3**, the resistance changes sharply due to the crystal structure transformation. During the subsequent cooling of the samples, the $R(T)$ dependences again obey the exponential law, but with an activation energy greater than that before the crystal structure transformation. It is

noteworthy that the conduction activation energies for the desolvated samples of complexes **2** and **3** are close, indicating that the desolvated complexes are also isostructural. It should be noted that the conductivity of complexes **1**–**3** is about one order of magnitude lower than the conductivity of TCNQ salts with cationic Mn(III) complexes with mononohalogen-substituted ligands 5-Hal-sal$_2$323 (Hal = Cl, Br).[29] The conductivity of TCNQ salts is strongly dependent on the character of the packing of anion-radicals in TCNQ stacks, which is determined by the shape, size and charge of the counterion.[33–37] TCNQ salts with large bulk cations generally exhibit low conductivity. It can be expected that the TCNQ salt with a cationic Mn(III) complex containing the unsubstituted ligand sal$_2$323 will have a higher conductivity than salts **1**–**3**.
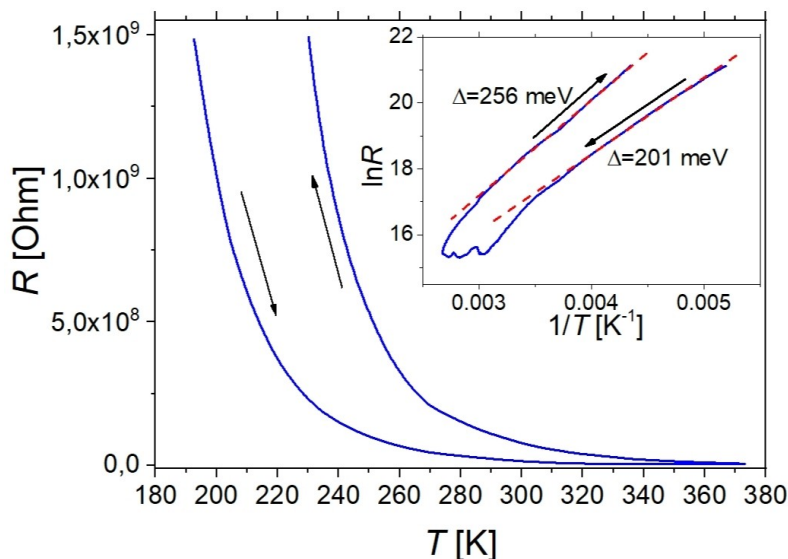
EurJIC
European Journal of Inorganic Chemistry

Research Article
doi.org/10.1002/ejic.202300749

Chemistry Europe
European Chemical Societies Publishing

Figure 9. The temperature dependence of the resistance R for the sample of complex **3**.

Conclusions

The 3,5-dihalide derivatives of the ligand sal_2323 (N,N′-bis(3-(2-oxy-benzylideneamino)propyl)-ethylenediamine) were used to synthesize cationic Mn(III) complexes with TCNQ electroactive anions. As a result, the ion-pair $[Mn(3,5\text{-}diCl\text{-}sal_2323)](TCNQ)_2$ (**1**) and $[Mn(3,5\text{-}X,Y\text{-}sal_2323)]_2(TCNQ)_3 \cdot 6CH_3CN$ (X,Y=Br, Br (**2**), X,Y=Br, Cl (**3**)) complexes combining spin transitions and electrical conductivity associated with the cationic and anionic subsystems, respectively, were obtained. The study of magnetic properties showed that complex **1** undergoes a incomplete spin transition from a low spin (LS) state (S=1) at 100 K to a high spin (HS) state (S=2) at heating up to 400 K without any hysteresis in heating and cooling modes. According to the X-ray diffraction analysis, temperature increase up to 373 K leads to elongation of Mn—N bonds and distortions of Mn(III) octahedral coordination, which are characteristic for the family of Mn(III) complexes with sal_2323 -ligands at the transition from LS to HS state. In contrast to **1**, isostructural complexes **2** and **3** contain 6 molecules of solvent acetonitrile, which is lost upon heating to 375 and 355 K, respectively, that is manifested by the appearance of a maximum at these temperatures on the DSC curves of the complexes. The loss of solvent leads to sharp jumps in the dependences of $\chi_m T$ vs T, resulting in the value of $\chi_m T$ reaching of 6.0 cm³ K/mol, which corresponds to the sum of $\chi_m T$ for two Mn(III) ions in the HS state. The loss of solvent is accompanied by the crystal structure transformation. Upon subsequent cooling from 400 K, a gradual reversible transition from the HS to the LS state is observed at low temperatures. The conductivity of complexes **1–3** at room temperature is $\sim 10^{-5}$–10^{-6} $Ohm^{-1} \cdot cm^{-1}$. The low conductivity values are due to the strong electronic localization on separate TCNQ radical-anions in the structure of **1** and the absence of continuous stacks of fractionally charged radical-anions in **2** and **3**. The loss of solvent at elevated temperatures in crystals **2** and **3** leads to resistance jumps in their temperature dependences of resistance.

Experimental Section

Materials and Analytical Methods

ACS reagent grade solvents (acetonitrile and 96% ethanol) were used without further purification. Reactants 3,5-diCl-salicylaldehyde, 3,5-diBr-salicylaldehyde, 3,5-Br,Cl- salicylaldehyde, N,N′-bis(3-aminopropyl)ethylenediamine, $Mn(ClO_4)_2 \cdot 6H_2O$, LiI, and 7,7,8,8-tetracyanoquinodimethane were purchased from various chemical sources and used as received except for the last one, which was recrystallized from acetonitrile. The LiTCNQ was synthesized following the literature methodology.[37] The starting perchlorates of $[Mn(3,5\text{-}diCl\text{-}sal_2323]^+$, $[Mn(3,5\text{-}diBr\text{-}sal_2323]^+$, and $[Mn(3,5\text{-}Br,Cl\text{-}sal_2323]^+$ were prepared according to procedure reported for $[Mn(3,5\text{-}diBr\text{-}sal_2323]ClO_4,^{[38]}$ using 96% ethanol as solvent in our syntheses. IR spectra were recorded on solid samples using a Bruker ALPHA spectrometer with the attenuated total reflectance (ATR) module. Elemental analyses were performed on a Vario MICRO cube (Elementar Analysensysteme GmbH, Langenselbold, Germany) equipment. Thermogravimetric analysis was carried out in a helium flow with a purity of 99.9999% using a STA 449 F3 Jupiter thermal analyzer. The heating rate was 2.0°C/min. Electron-probe X-ray microanalysis (EPMA) was performed with a Zeiss Supra-25 analytical field emission electron microscope equipped with a Gemini electron optical column at a magnification varying from 600 to 6200 depending on the sample and the electron beam energy of 9.7–20 keV. The effective analysis depth was 1–3 μm.

Synthesis of Complexes

[Mn(3,5-diCl-sal₂323)]⁺(TCNQ)₂ (1)

The hot solution of TCNQ (0.03 mmol, 0.0061 g) and LiTCNQ (0.03 mmol, 0.0063 g) in 15 ml of acetonitrile was added to the hot solution of $[Mn(3,5\text{-}diCl\text{-}sal_2323)]ClO_4$ (0.03 mmol, 0.0202 g) in 5 ml

EurJIC
European Journal of Inorganic Chemistry

Research Article
doi.org/10.1002/ejic.202300749

Chemistry
Europe

European Chemical
Societies Publishing

of acetonitrile. The resulting solution was stirred well for about 15 minutes and then was cooled slowly to −10 °C in refrigerator. Shiny black crystals were formed within a week that were recovered by filtration and washed with cold acetonitrile. Yield: 40.8%. Elemental analysis, calc. (%) for $C_{46}H_{32}Cl_4MnN_{12}O_2$: C, 56.29, H, 3.29, N, 17.12; found: C, 55.58, H, 3.27, N, 16.90. The EPMA microanalysis afforded the elements ratio Mn:Cl = 1:4. IR spectrum (cm^{-1}), ν(C≡N): 2165, 2150; ν(C=N): 1617 (Figure S15).

[Mn(3,5-diBr-sal₂323)]₂(TCNQ)₃·6CH₃CN (2)

The hot solution of TCNQ (0.02 mmol, 0.0041 g) and LiTCNQ (0.02 mmol, 0.0042 g) in 15 ml of acetonitrile was added to the hot solution of [Mn(3,5-diBr-sal₂323)]ClO₄ (0.04 mmol, 0.0340 g) in 5 ml of acetonitrile. The resulting solution was stirred well for about 15 minutes and then was cooled slowly to −10 °C in refrigerator. Shiny black crystals were formed within a week that were recovered by filtration and washed with cold acetonitrile. Yield: 53.2%. Elemental analysis, calc. (%) for $C_{84}H_{66}Br_8Mn_2N_{22}O_4$ ([Mn(3,5-diBr-sal₂323)]₂(TCNQ)₃·2CH₃CN): C, 45.93, H, 3.03, N, 14.03; found: C, 45.80, H, 3.20, N, 14.09. The EPMA microanalysis afforded the elements ratio Mn:Br = 1:4. Elemental analysis shows that storing the complex in air leads to the loss of 4 molecules of lattice acetonitrile. IR spectrum (cm^{-1}), ν(C≡N): 2198, 2162, 2150; ν(C=N): 1598, 1563 (Figure S8). After heating to 400 K, complex **2** loses the solvated acetonitrile (Figure S1) and experiences a crystal structure transformation. IR spectrum desolvated complex (cm^{-1}), ν(C≡N): 2202, 2165, 2140; ν(C=N): 1631 (Figure S9). Comparison of IR spectra of complex **2** before (orange) and after (green) heating to 400 K is presented in Figure S10.

Mn(3,5-Br,Cl-sal₂323)]₂(TCNQ)₃·6CH₃CN (3)

The synthesis was carried out similarly to **1**, using 0.03 mmol of [Mn(3,5-Br,Cl-sal₂323)]ClO₄ instead of [Mn(3,5-diCl-sal₂323)]ClO₄. Yield: 73.4%. Elemental analysis, calc. (%) for $C_{84}H_{66}Cl_4Br_4Mn_2N_{22}O_4$ (Mn(3,5-Br,Cl-sal₂323)]₂(TCNQ)₃·2CH₃CN): C, 49.97, H, 3.29, N, 15.26; found: C, 49.39, H, 3.30, N, 15.54. The EPMA microanalysis afforded the elements ratio Cl:Mn:Br = 2:1:2. Elemental analysis shows that storing the complex in air leads to the loss of 4 molecules of lattice acetonitrile. IR spectrum (cm^{-1}), ν(C≡N): 2200, 2162, 2155; ν(C=N): 1562 (Figure S11),. After heating to 400 K, complex **3** loses the solvated acetonitrile (Figure S2) and experiences a crystal structure transformation. IR spectrum desolvated complex (cm^{-1}), ν(C≡N): 2203, 2165, 2145; ν(C=N): 1605 (Figure S12). Comparison of IR spectra of complex **3** before (orange) and after (green) heating to 400 K is presented in Figure S13.

X-ray Crystallography

X-ray data for single crystal **1–3** were collected on an Agilent XCalibur CCD diffractometer with an EOS detector (Agilent Technologies UK Ltd, Yarnton, Oxfordshire, England) at four temperatures 100, 200, 300 and 373 K for **1** and at 100 K for **2** and **3** using graphite monochromatized MoK$_\alpha$ radiation (λ = 0.71073 Å). Structures were solved by direct methods and refined from all F^2 data by SHELXTL program suite.[39] All non-hydrogen atoms were refined with anisotropic thermal parameters, the positions of hydrogen atoms were obtained from Fourier difference syntheses and refined with the with riding model constraints. The X-ray crystal structure data were deposited with the Cambridge Crystallographic Data Center. Deposition numbers 2307583 (for **1**, 100 K), 2307584 (for **1**, 200 K), 2307585 (for **1**, 300 K), 2307586 (for **1**, 373 K), 2307587 (for **2**, 100 K) and 2307588 (for **3**, 100 K) contain the supplementary crystallographic data for this paper. These data are provided free of charge by the joint Cambridge Crystallographic Data Centre and Fachinformationszentrum Karlsruhe Access Structures service. Selected crystallographic parameters, as well as the statistics of data collection and refinement, are shown in Table S1.

Magnetic Measurement

The temperature dependencies of molar magnetic susceptibility χ(T) for powdered samples **1–3** were measured in static magnetic field 5 kOe by a vibrating-sample magnetometer of a Cryogen Free Measurement System (Cryogenic Ltd, UK). The change of χ value during the thermal cycle at relatively slow heating/cooling rates ~2 K/min in the temperature range of 2–400 K was established. The freshly prepared samples were placed in a magnetometer at room temperature. After that, the χ(T) dependence was measured during the first cooling cycle from T = 300 K to 2 K. Then χ vs. T measurement was immediately started during heating from T = 2 K to 400 K (second cycle). The third and fourth thermal cycles were samples cooling/heating also in an extended temperature range of 400 K– 2 K–400 K.

Transport Measurement

The temperature dependence of the electrical resistance of single crystals was measured using a two-probe method by the multimeter with high input impedance. The contacts were made using the conducting graphite paste. In the control experiments we have measured the in-plane resistance at 300 K by four-probe technique using the Lock-in amplifier with the input impedance 100 MOhm, when the sample resistance was comparatively small, and we have found that the result did not differ considerably from that obtained by the two-probe geometry, i.e. the contact resistance was smaller than the resistance of the sample. The samples **1** had the shape of the plate with the size 0.5×0.35×0.1 mm^3, samples **2** and **3** were thin like-needles with characteristic sizes about 1.0×0.1×0.05 mm^3. Resistance measurements were always carried out along the longest axis of single crystals (a-axis), i.e., in the direction coinciding in the case of complex **1** with the propagation of the TCNQ–C chains or in the plane of the TCNQ layers in the structure of complexes **2** and **3**. The error in the conductivity calculations was about 40% and was associated mainly with the fact that the shapes of the samples were far from ideal rectangular plates or well-defined needles.

Acknowledgements

Conflict of Interests

The authors declare no conflict of interest.

Eur. J. Inorg. Chem. **2024**, e202300749 (10 of 11)

© 2024 Wiley-VCH GmbH

Data Availability Statement

The data that support the findings of this study are available in the supplementary material of this article.

[1] L. Ouahab, *Multifunctional Molecular Materials*, Pan Stanford Publishing, Singapore, **2013**, p. 316.

[2] L. Valade, I. Malfant, C. Faulmann, *In Multifunctional Molecular Materials* (Ed.: L. Ouahab) Pan Stanford Publishing, Pte. Ltd.: Singapore, **2013**, pp. 163–174.

[3] O. Sato, Z.-Y. Li, Z.-S. Yao, S. Kang, S. Kanegawa, *In Spin-Crossover Materials: Properties and Applications* (Ed.: M. A. Halcrow), John Wiley & Sons, Oxford, **2013**, pp. 304–319.

[4] Ö. Üngör, E. S. Choi, M. Shatruk, *Chem. Sci.* **2021**, *12*, 10765 and references therein.

[5] C. Faulmann, K. Jacob, S. Dorbes, S. Lampert, I. Malfant, M. L. Doublet, L. Valade, J. A. Real, *Inorg. Chem.* **2007**, *46*, 8548–8559.

[6] K. Takahashi, H. B. Cui, Y. Okano, H. Kobayashi, H. Mori, H. Tajima, Y. Einaga, O. Sato, *J. Am. Chem. Soc.* **2008**, *130*, 6688–6689.

[7] K. Takahashi, H. B. Cui, Y. Okano, H. Kobayashi, Y. Einaga, O. Sato, *Inorg. Chem.* **2006**, *45*, 5739–5741.

[8] Y. N. Shvachko, D. V. Starichenko, A. V. Korolyov, A. I. Kotov, L. I. Buravov, V. N. Zverev, S. V. Simonov, L. V. Zorina, E. B. Yagubskii, *Magnetochemistry* **2017**, *3*, 9.

[9] H. Phan, S. M. Benjamin, E. Steven, J. S. Brooks, M. Shatruk, *Angew. Chem. Int. Ed.* **2015**, *54*, 823–827.

[10] Y. N. Shvachko, D. V. Starichenko, A. V. Korolyov, E. B. Yagubskii, A. I. Kotov, L. I. Buravov, K. A. Lyssenko, V. N. Zverev, S. V. Simonov, L. V. Zorina, O. G. Shakirova, L. G. Lavrenova, *Inorg. Chem.* **2016**, *55*, 9121–9130.

[11] Ö. Üngör, E. S. Choi, M. Shatruk, *Eur. J. Inorg. Chem.* **2021**, 4812–4820.

[12] O. A. Qamar, F. Jamil, M. Hussain, M. Mustafa, R. U. Rehman, A. Inayat, M. S. Habib, M. Sajid, *Chem. Pap.* **2023**, https://doi.org/10.1007/s11696-023-03017-6.

[13] P. Getlich, in *Spin Crossover in Transition Metal Compounds I* (Eds.: H. A. Goodwin), Springer, Berlin, **2004**, pp. 1–324.

[14] M. A. Halcrow, Ed., *Spin-Crossover Materials*: Properties and Applications, Wiley, Oxford, **2013**, pp. 1–564.

[15] S. Brooker, *Chem. Soc. Rev.* **2015**, *44*, 2880–2892.

[16] G. G. Morgan, K. D. Murnaghan, H. Meller-Bunz, V. McKee, C. J. Harding, G. G. Morgan, K. D. Murnaghan, H. Muller-Bunz, V. Mckee and C. J. Harding, *Angew. Chem. Int. Ed.* **2006**, *45*, 7192–7195; *Angew. Chem.* **2006**, *118*, 7350–7353.

[17] J. Olguin, *Coord. Chem. Rev.* **2020**, *407*, 213148–213177 and references therein.

[18] M. M. Harris, I. A. Kühne, C. T. Kelly, V. B. Jakobsen, R. Jordan, L. O'Brien, H. Müller-Bunz, S. Felton, G. G. Morgan, *Cryst. Growth Des.* **2023**, *23*, 3996–4012.

[19] S. Bagchi, S. Kamilya, S. Mehta, S. Mandal, A. Bandyopadhyay, A. Narayan, S. Ghosh, A. Mondal, *Dalton Trans.* **2023**, *52*, 11335–11348.

[20] A. J. Fitzpatrick, E. Trzop, H. Meller-Bunz, M. M. Dirtu, Y. Garcia, E. Collet, G. G. Morgan, *Chem. Commun.* **2015**, *51*, 17540–17543.

[21] S. Wang, Y.-J. Li, F.-F. Ju, W.-T. Xu, K. Kagesawa, Y.-H. Li, M. Yamashita, W. Huang, *Dalton Trans.* **2017**, *46*, 11063–11077.

[22] S. Ghosh, S. Bagchi, S. Kamilya, A. Mondal, *Dalton Trans.* **2020**, *49*, 14776–14780.

[23] V. B. Jakobsen, E. Trzop, L. C. Gavin, E. Dobbelaar, S. Chikara, X. Ding, K. Esien, H. Muller-Bunz, S. Felton, V. S. Zapf, E. Collet, M. A. Carpenter, G. G. Morgan, *Angew. Chem. Int. Ed.* **2020**, *59*, 13305–13312; *Angew. Chem.* **2020**, *132*, 13407–13414.

[24] S. Ghosh, S. Bagchi, S. Kamilya, A. Mondal, *Dalton Trans.* **2021**, *50*, 4634–4642.

[25] A. V. Tiunova, A. V. Kazakova, D. V. Korchagin, G. V. Shilov, L. V. Zorina, S. V. Simonov, K. V. Zakharov, A. N. Vasiliev, E. B. Yagubskii, *Chem. Eur. J.* **2021**, *27*, 17609–17619.

[26] V. B. Jakobsen, E. Trzop, E. Dobbelaar, L. C. Gavin, S. Chikara, X. Ding, M. Lee, K. Esien, H. Muller-Bunz, S. Felton, E. Collet, M. A. Carpenter, V. S. Zapf, G. G. Morgan, *J. Am. Chem. Soc.* **2022**, *144*, 195–211.

[27] E. Dobbelaar, V. B. Jakobsen, E. Trzop, M. Lee, S. Chikara, X. Ding, H. Muller-Bunz, K. Esien, S. Felton, M. A. Carpenter, E. Collet, G. G. Morgan, V. S. Zapf, *Angew. Chem. Int. Ed.* **2022**, *61*, e202114021.

[28] V. B. Jakobsen, S. Chikara, J.-X. Yu, E. Dobbelaar, C. T. Kelly, X. Ding, F. Weickert, E. Trzop, E. Collet, H.-P. Cheng, G. G. Morgan, V. S. Zapf, *Inorg. Chem.* **2021**, *60*, 6167–6175.

[29] A. V. Kazakova, A. V. Tiunova, D. V. Korchagin, G. V. Shilov, E. B. Yagubskii, V. N. Zverev, S. C. Yang, J.-Y. Lin, J.-F. Lee, O. V. Maximova, A. N. Vasiliev, *Chem. Eur. J.* **2019**, *25*, 10204–10213.

[30] H. Endres, in *Extended Linear Chain Compounds*, Vol. 3 (ed. J. S. Miller), Plenum, **1983**, pp. 263–317.

[31] F. H. Herbstein, M. Kapon, *Crystallogr. Rev.* **2008**, *14*, 3–74.

[32] T. J. Kistenmacher, T. J. Emge, A. N. Bloch, D. O. Cowan, *Acta Crystallogr. Sect. B* **1982**, *38*, 1193–1199.

[33] J. L. Brédas, J. P. Calbert, D. A. da Silva Filho, J. Cornil, *Proc. Natl. Acad. Sci. USA* **2002**, *99*, 5804–5809.

[34] Ö. Üngör, M. Shatruk, *Polyhedron* **2020**, *177*, 114254.

[35] W. J. Siemons, P. E. Bierstedt, R. G. Kepler, *J. Chem. Phys.* **1963**, *39*, 3523–3528.

[36] I. F. Shchegolev, *Phys. Status Solidi A* **1972**, *12*, 9–45.

[37] L. Melby, R. Harder, W. Hertler, W. Mahler, R. Benson, W. Mochel, *J. Am. Chem. Soc.* **1962**, *84*, 3374.

[38] K. Pandurangan, B. Gildea, C. Murray, C. J. Harding, H. Müller-Bunz, G. G. Morgan, *Chem. Eur. J.* **2012**, *18*, 2021–2029.

[39] G. M. Sheldrick, *Acta Crystallogr.* **2015**, *C71*, 3–8.

RESEARCH ARTICLE

The new bifunctional salts [Mn(III)(3,5-diHal-sal₂323)]ₖ(TCNQ)ₗ(CH₃CN)ₘ have been synthesized. An incomplete spin transition is observed in the diCl derivative. Isostructural Cl,Br and diBr salts contain six solvated acetonitrile molecules, which are lost upon heating, accompanied by the irreversible crystal structure transformation and abrupt transition to the HS state.

1: X = Y = Cl **2**: X = Y = Br
k=1,l=2,m=0   k=2,l=3,m=6
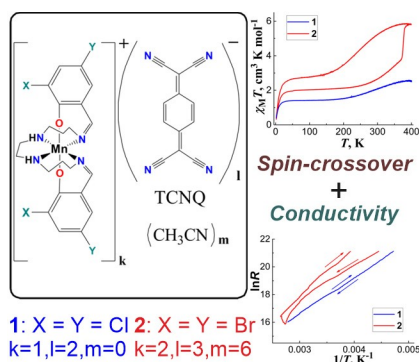
A. V. Tiunova, D. V. Korchagin*, A. V. Kazakova*, G. V. Shilov, L. I. Buravov, A. I. Dmitriev, M. V. Zhidkov, V. N. Zverev, E. B. Yagubskii*, S. M. Aldoshin

1 – 12

Solvent and Dihalide Substituent Effects on Crystal Structure, Spin-Crossover Behavior and Conductivity of the Cationic Mn(III) Complexes with Electroactive TCNQ Counteranions